

A Generalizable Theory for the Reynolds Stress, Based on the Lagrangian Turbulence Transport

T.-W. Lee

Mechanical and Aerospace Engineering, SEMTE, Arizona State University, Tempe, AZ, 85287

Abstract- Using the Lagrangian transport of momentum, the Reynolds shear stress can be expressed in terms of basic turbulence parameters. In this view, the Reynolds stress gradient represents the lateral transport of streamwise momentum, balanced by the u'^2 transport, pressure and shear force terms in the momentum equation. We extend this formalism to other turbulence parameters such as diagonal components of the Reynolds stress, and also to more complex flows (boundary layer flows with adverse pressure gradients and pipe flows with swirl). Data from direct numerical simulations (DNS) are used to validate this full set of turbulent transport equations, exhibiting a good degree of consistency and agreement for all of the components and across different geometries. An example of the use of this full set of turbulence transport equations is shown for turbulent jet flows.

T.-W. Lee

Mechanical and Aerospace Engineering, SEMTE

Arizona State University

Tempe, AZ 85287-6106

Email: attwl@asu.edu

INTRODUCTION

Determination of the Reynolds stress in terms of root turbulence parameters has profound implications in fluid physics and engineering, as its shear stress component adds to the mean momentum structure. For some simple geometries such as fully-developed pipe flow, prescription of the Reynolds shear stress results directly in the mean velocity profile.

$$\mu \frac{d^2 U}{dy^2} = \frac{dP}{dx} + \rho \frac{d(u'v')}{dy} \quad (1)$$

It can be said that determination of the Reynolds stress is central to solving the turbulence problem. Since many scientific and engineering phenomena involve turbulent flows, different ways of expressing the Reynolds stress in terms of known (or computable) parameters have been devised so that artificial closure is achieved, with varying degrees of success (or inadequacy, depending on one's perspective). The procedure is typically to expand the Reynolds stress or the “turbulence viscosity”, in terms of higher-order terms, e.g. turbulence kinetic energy, dissipation, and third-order correlations in the case of Reynolds stress models. In turn, these higher-order terms need to be algebraically modelled as reviewed in some articles [1-6]. The models are quite diverse at times complex, and we defer to these references since the current approach has no bearing on the existing methods.

Recently, we have developed a new formulation for the Reynolds stress based on the Galilean-transformed Navier-Stokes equation [7-9], where a simple, explicit expression is derived for the gradient of the Reynolds shear stress, as shown below:

$$\frac{d(u'v')}{dy} = -C_1 U \left[\frac{d(u'^2)}{dy} + \frac{1}{\rho} \frac{d|P|}{dy} \right] + v \frac{d^2 u'}{dy^2} \quad (2)$$

The derivation can be found in Refs. 7-9, and an expanded version below. Eq. 2 is an expression arising from the momentum balance for a control volume moving at the local mean velocity, where the Reynolds shear stress represents the lateral (y-direction) transport of u' momentum [7-9]. This lateral transport is balanced by the longitudinal transport and force terms on the right-hand side (RHS) of Eq. 2, where the d/dx gradients are transformed to d/dy , following the displacement of the fluid [9]. Viscous shear stress due to gradient of the turbulent fluctuation velocity ($u' = u'_{rms}$) is a new concept; however, we visualize that if there exists a gradient in the mean fluctuation velocity then it will lead to shear stress in the mean in this moving coordinate frame. The shear stress from the mean velocity is considered to be negligible in comparison to this “turbulent shear stress”. Once we have the gradient from Eq. 2, then the Reynolds stress itself can be obtained through numerical or algebraic integration. For example, for rectangular channel flows we can integrate Eq. 1 by parts:

$$\langle u'v' \rangle = -C_1 \left[U u'^2 - \int_0^y u'^2 \frac{dU}{dy} dy \right] + v \frac{du'_{rms}}{dy} \quad (3)$$

This approach has proven to work quite well, insofar as prescribing the Reynolds shear stress, for channel, boundary layer and jet flows [7-9]. We can see that in order to solve for $u'v'$ we introduce

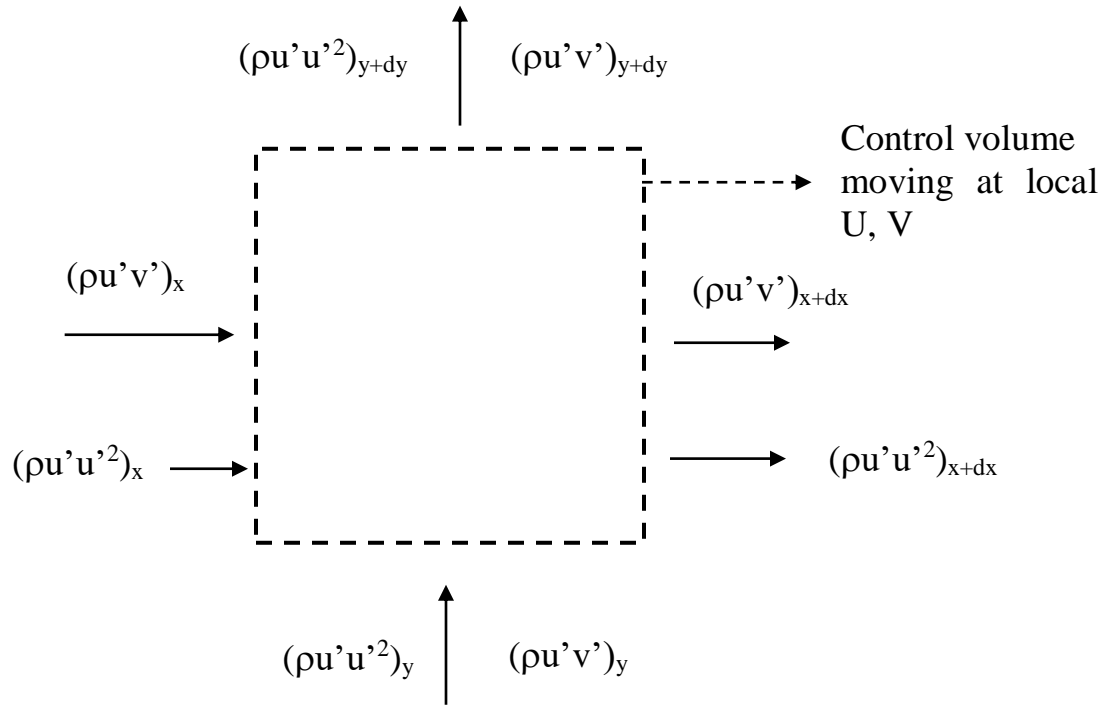
yet another turbulence parameter, u'^2 . A similar transport equation has been developed, to simultaneously solve for u'^2 , $u'v'$ and U in jet flows [9].

The current formulation is based on momentum conservation principle (in a non-stationary coordinate frame), so that the resulting expression for the Reynolds stress (Eq. 2) contains, and also reveals, the transport processes leading to the turbulence shear stress. For the same reason, it may be possible to generalize this approach to other more complex geometries. In this work, we show that this approach can indeed be applied to pipe flow with swirl and boundary-layer flows with adverse pressure gradients, and its turbulence momentum balance checked with DNS (direct numerical simulation) data. Moreover, we extend the Lagrangian transport formalism to other turbulence variables, u'^2 and v'^2 , so that the complete Reynolds stress tensor (diagonal and off-diagonal terms) can be determined. This extension produces a full set of transport equations for the Reynolds stress components, so that relatively simple numerical integration can be performed in conjunction with the Reynolds-averaged Navier-Stokes equation (RANS, e.g. Eq. 1) to solve for the turbulent flow structure. Comparisons are made with DNS and experimental data to support the unique hypotheses embodied in the current formalism.

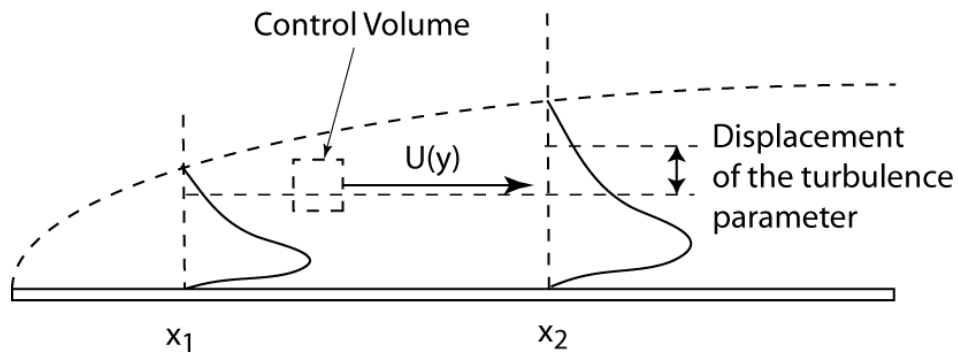
LAGRANGIAN TURBULENCE TRANSPORT

We can visualize a control volume moving at the local mean velocity, U and V , so that the effects of turbulence fluctuation components (the Reynolds stress) are isolated, as shown in Fig. 1. Eq. 2 is the transport equation for u' which has already been described [7-9], so we consider two new transport equations for v' and u'^2 as shown in Fig. 1. If the current formalism did not

lead to the correct transport balance for these components, then something would be amiss and we also need these additional variables since they appear in Eq. 2.



(a)



(b)

Fig. 1. Schematics of the dynamics contained in Eq. 2. (a) y -momentum (v') and longitudinal kinetic energy balance (u'^2) following a control volume, which is moving at the local mean velocity; and (b) the displacement concept leading to $d/dx \rightarrow d/dy$.

Then, the transport equations for v' (lateral turbulence momentum) and u'^2 (longitudinal turbulence kinetic energy) in the current coordinate frame are:

$$\frac{d(u'v')}{dx} + \frac{d(v'^2)}{dy} = -\frac{1}{\rho} \frac{dP}{dy} + \nu \frac{d^2 v_{rms}}{dy^2} \quad (4)$$

$$\frac{d(u'^2 u')}{dx} + \frac{d(u'^2 v')}{dy} = \frac{d(Pu')}{dx} + 2\nu \left(\frac{du'}{dy}\right)^2 \quad (5)$$

Now, we make the same d/dx to d/dy transform, which was used to arrive at Eq. 2. This is based on the displacement concept as shown in Fig. 1(b) and in our previous work [7-9]. We list all the hypotheses involved as below.

$$\text{Hypothesis 1: } \frac{d}{dy} \rightarrow \pm CU \frac{d}{dy} \quad (6),$$

where C is constant with the order of magnitude as $\sim 1/U_{ref}$. The sign depends on the flow geometry. There are no displacement effects for channel flows. However, we still obtain the above conversion in the spatial gradients using the “probe transform”. A brief algebra of this transform is shown in the Appendix. Implicit in this hypothesis is that the both the vectors (u' , v') and scalars (pressure, u'^2) are transformed in this manner.

The above transport equations contain the dreaded triple correlation(s). For Lagrangian transport, a second hypothesis is used for the triple correlations as below, and validated later with DNS data.

$$\text{Hypothesis 2: } u'^2 v' \approx u' \cdot u' v', \quad u' v'^2 \approx v' \cdot u' v', \text{ etc.} \quad (7)$$

This simplistic product rule leads to unexpected results for u'^2 profile, as discussed in the next section. The second of the above triple product appears in Eq. 5 when the pressure is written as below.

$$\text{Hypothesis 3: } P \approx -\rho v'^2 \quad (8)$$

For channel flows, this relation is exact [10], and we apply it as an approximation for boundary layer flows with and without adverse pressure gradient, and the results are discussed below. As noted above, using this pressure expression leads to $u' v'^2$ in Eq. 5, which is converted to $v'(u' v')$ via hypothesis 2 (Eq. 7). This at first appears to be an over-simplification, but leads to some unexpected results within the current Lagrangian formalism, as discussed below.

$$\text{Hypothesis 4: } \textit{Pressure work} \approx \frac{d(Pu')}{dx} \quad (9)$$

These are evidently new and unique concepts, nonetheless we proceed to write the following turbulence transport equations using the above hypotheses. We already showed the transport equation for $d(u' v')/dy$ in Eq. 2, and we just organize the constants in C_{ij} format.

$$\frac{d(u' v')}{dy} = -C_{11} U \frac{d(u'^2)}{dy} + C_{12} U \frac{dv'^2}{dy} + C_{13} \frac{d^2 u'}{dy^2} \quad (10)$$

$$\frac{d(v'^2)}{dy} = -C_{21}U \frac{d(u'v')}{dy} + C_{22}U \frac{dv'^2}{dy} + C_{23} \frac{d^2v_{rms}}{dy^2} \quad (11a)$$

Alternatively,

$$\frac{d(v'^2)}{dy} = \frac{-C_{21}U \frac{d(u'v')}{dy} + C_{23} \frac{d^2v_{rms}}{dy^2}}{1 - C_{22}U} \quad (11b)$$

$$\frac{d(u'^3)}{dy} = -C_{31} \frac{1}{U} \frac{d(u'v' \cdot u')}{dy} + C_{32} \frac{1}{U} \frac{d(v' \cdot u'v')}{dy} + C_{33} \left(\frac{du'}{dy} \right)^2 \quad (12)$$

C_{12} modifies the pressure term while absorbing the effect of density, and C_{13} constants are the kinematic viscosity, ν (C_{13} and C_{23}) or 2ν (C_{33}).

For boundary-layer flows with and without adverse pressure gradients, Eq. 10 can be used, without having to add any adjustment terms, wherein the pressure effect is manifest through $P \sim -\rho v'^2$ (hypothesis 3), i.e., C_{12} term. For axi-symmetric flows, containing swirl, we can similarly write the following turbulence momentum transport equation after properly vectorizing the gradients and centripetal pressure in cylindrical coordinates. To demonstrate the similarity in the logic, we write the gradient of the main Reynolds shear stress, $u_r'u_z'$.

$$\frac{d}{dr}(ru_r'u_z') = -A_{11}rU_{trans} \frac{d(u_z'^2)}{dr} + A_{12}rU_{trans} \frac{d(u_\theta'u_z')}{dr} + A_{13}rU_{trans} \frac{dP}{dr} + A_{14}r \frac{d}{dr} \left(r \frac{du_{z,rms}'}{dr} \right) \quad (13)$$

Here, the centripetal pressure is given by

$$\frac{dP}{dr} = -\rho \frac{U_\theta^2}{r} \quad (14)$$

The translational velocity in swirl flow is

$$U_{trans} = \sqrt{U_z^2 + U_\theta^2} \quad (15)$$

For u_r, u_θ , we have,

$$\frac{d}{dr}(ru_r' u_\theta') = -A_{21} r U_{trans} \frac{d(u_\theta'^2)}{dr} + A_{22} r U_{trans} \frac{d(u_\theta' u_z')}{dr} + A_{33} r U_{trans} \frac{dP}{dr} + A_{34} r \frac{d}{dr} \left(r \frac{du_{\theta,rms}'}{dr} \right) \quad (16)$$

Thus, the current formalism allows for extension to other geometries, and for derivation of the transport equations for all of the requisite turbulence variables. We demonstrate below its validity using available data.

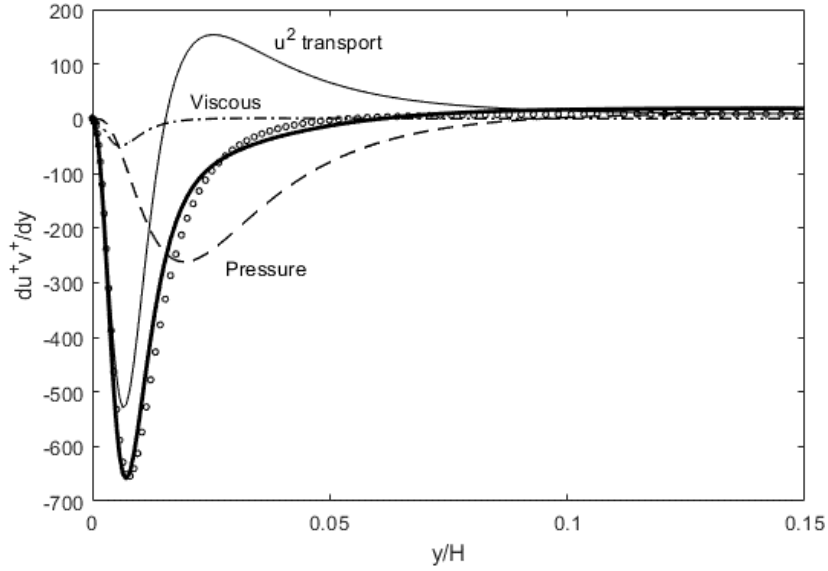
RESULTS AND DISCUSSION

A Full Set of Turbulent Transport Equations

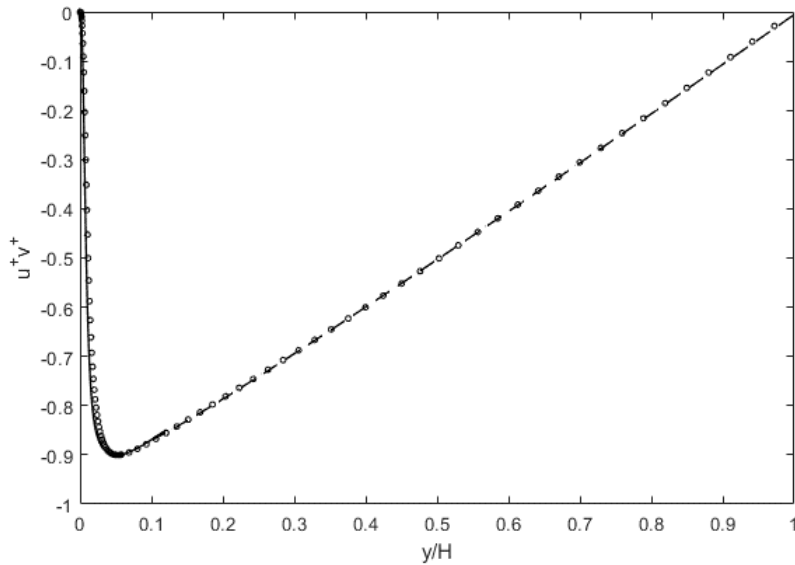
Let us examine the above full set of turbulence transport equations (Eqs. 10-12) for rectangular channel flows, for which high-fidelity DNS data are readily available, e.g. Graham et al. [11]. We

can start with the Reynolds shear stress gradient, du^+v^+/dy , as shown in Fig. 2(a). The + superscript indicates normalization by the friction velocity, as presented in Graham et al. [11]. The Reynolds stress budgets from Eqs. 10-12 are checked by inputting the DNS data on the RHS and computing the sum of all the terms from appropriated differentials. Then, the left-hand side (LHS) is evaluated separately from the DNS, and compared with the above sum from RHS. When this is done in Eq. 10, we can see that there is a very close agreement between the current theory and DNS data. As discussed in our earlier work [9], it is the triad of momentum terms, longitudinal transport, pressure and viscous forces, that leads the Reynolds shear stress. Thus, intuitively and theoretically, the Reynolds shear stress is determined by the fluctuating momentum components, particularly since $P = -\rho v^2$ in channel flows. We can integrate the gradient of the Reynolds shear stress thus obtained from Eq. 10, to compare directly with u^+v^+ , in Fig. 2(b). Although there is a good agreement between theory and DNS for the gradient in Fig. 2(a), any minute deviation can cause departure during numerical integration. Any error in the gradient causes trajectory deviations sending the integrated quantity in the wrong direction, resulting in accumulated discrepancy from the correct u^+v^+ . There are two remedies to reduce this kind of numerical error: one is to enforce the boundary condition at the other end (e.g. centerline) algebraically, while the second is to integrate from both ends (wall and the centerline) until the solution intersects. This is merely a numerical error correction scheme and stipulation of the boundary condition, and does not deduct from the theoretical integrity. For the Reynolds shear stress, we opt for the latter method since the small gradient near the centerline is benign to the numerical integration, and can be used for a large section of the channel flow. This “back” integration (inbound from the centerline) is plotted as a dashed line in Fig. 2(b), while the “forward” integration (outbound from the wall) is plotted as a solid line. Comparison with DNS data is quite good, using the above dual

integration scheme. Due to the large negative gradient involved near the wall, the forward integration starts to deviate at y/H of only 0.15 and back-integrated solution is used aft of that point.



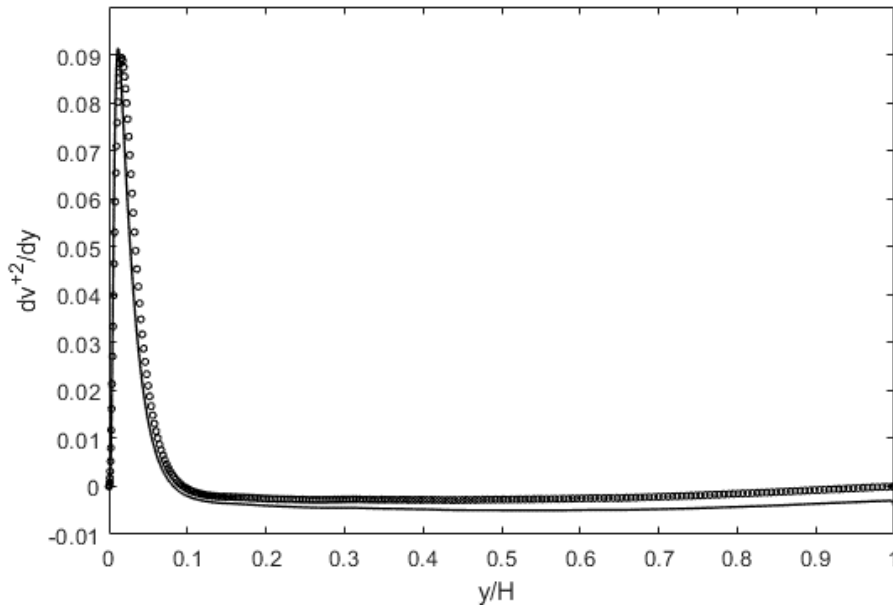
(a)



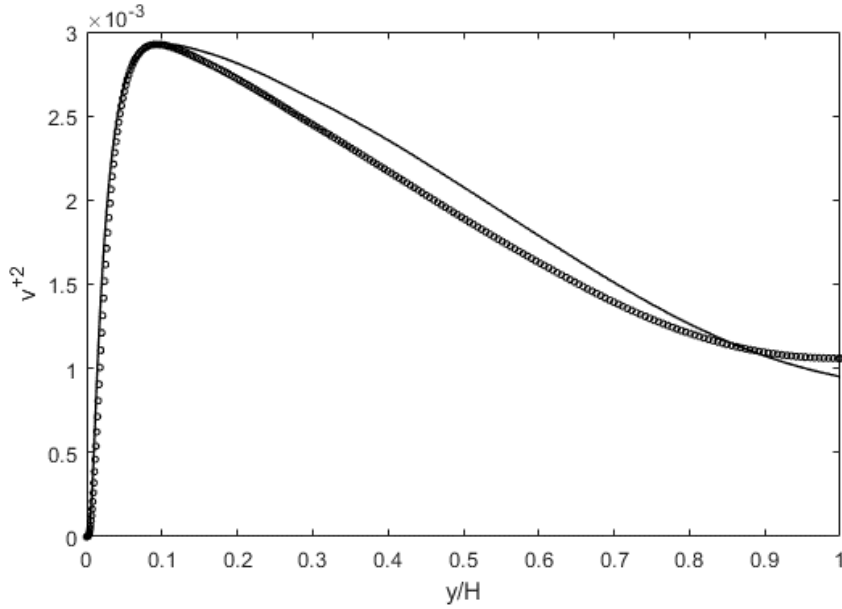
(b)

Fig. 2. (a) Reynolds shear stress gradient budget (a) for channel flows, consisting of u'^2 transport, viscous and pressure terms in Eq. 10; and (b) Comparison of $u^+ v^+$, obtained from numerical integration of Eq. 10, with DNS data [11].

For the lateral fluctuating momentum flux, v^{+2} , we plot its gradient in Fig. 3(a). Although the gradient is obtained using Eq. 11 is structurally correct, the accuracy is not as good as the previous example for du^+v^+/dy . We can see that the gradient for v^{+2} is about much smaller in magnitude than du^+v^+/dy , thus relative numerical accuracy is reduced during computation of the gradient terms. Also, the slope does not quite reach zero at the centerline. Nonetheless, we can still integrate and again compare directly with DNS, in Fig. 3(b). The centerline boundary condition is again enforced, by using a correction function of the form, $(v^{+2})_{\text{corr}} = (v^{+2})_{\text{integrated}} + c_v(y/H)$. A linear function of y/H is added to integrated v^{+2} , where $c_v = \Delta v^{+2}$ = deviation of the $(v^{+2})_{\text{integrated}}$ from v^{+2} at $y/H=1$. This will ensure that centerline v^{+2} is reached, or close in this case, at $y/H=1$. Then, the agreement is acceptable, as shown in Fig. 3(b).



(a)

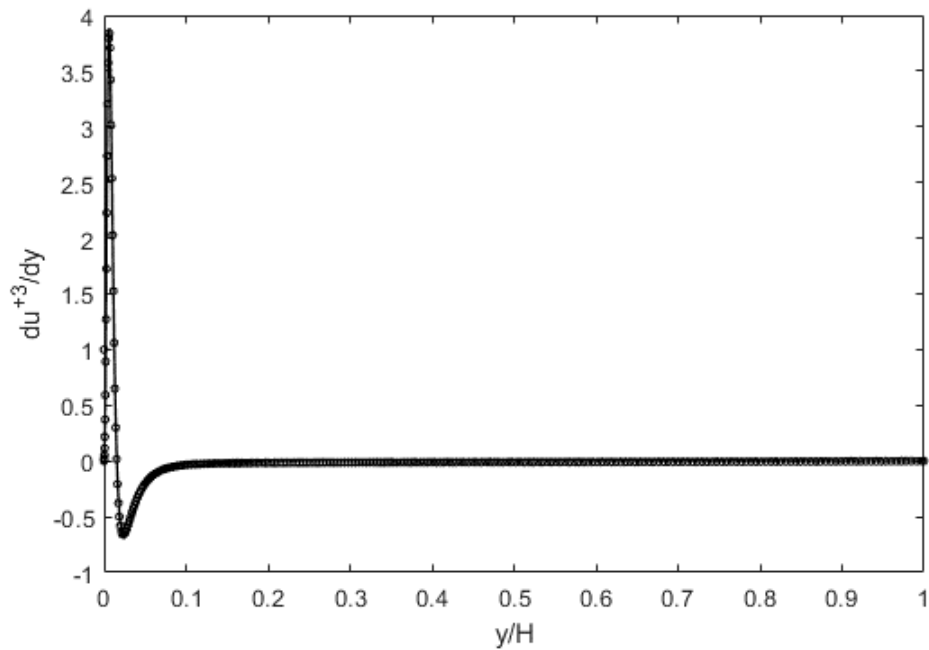


(b)

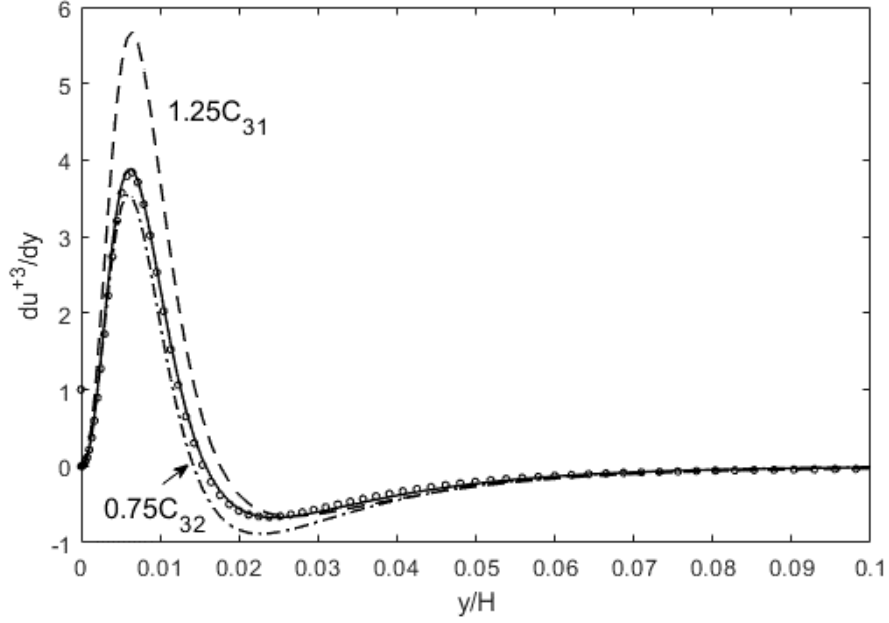
Fig. 3. (a) dv^{+2}/dy budget for channel flows from Eq. 11; and (b) comparison of v^{+2} , obtained from numerical integration of Eq. 11, with DNS data [11].

For the gradient of the longitudinal kinetic energy flux, du^{+3}/dy , the agreement between the theory (Eq. 12) and DNS-derived result is almost exact in Fig. 4(a), somewhat unexpected due to the approximation, $u^{+2}v^{+}=u^{+}(u^{+}v^{+})$, in from Eq. 7. This prompts further scrutiny. We zoom in on the near-wall region ($y/H=0 \sim 0.1$), and also vary the parameters in Eq. 12, C_{31} and C_{32} , relatively to what resulted in the theoretical line in Fig. 4(a). The re-calculated gradients are shown in Fig. 4(b), along with the original theoretical (solid) line which exhibits very close tracking of the DNS gradient even upon close inspection. Variations of the constants, C_{31} and C_{32} , alters the u^{+3} gradient, where C_{31} determines the near-wall peak while C_{32} causes the variation in the secondary “dip” in the gradient. This brief exercise confirms the effectiveness of the u^{+2} balance expressed by Eq. 12, but also reveals the dynamics involved in “turbulence production”, including the

$u^{+2}v^+=u^+(u^+v^+)$ hypothesis. The near-wall peak evidently means that the x-component of the turbulent kinetic energy, u^{+2} , increases quite sharply there. The sensitivity of this peak to C_{31} indicates that that term, $du^{+2}v^+/dy$, is mainly responsible for this surge. Recalling that this is the transport of u^{+2} due to vertical fluctuation, v^+ , it is the lateral “migration” of u^{+2} that results in a large accumulation of turbulence kinetic energy close to the wall. The secondary dip, then, is due to the pressure work term, suggesting that the built-up kinetic energy is consumed by the pressure work term and thus distributing it toward the centerline. In summary, the Lagrangian transport analysis simply and accurately presents the underlying dynamics of Reynolds stress and turbulent kinetic energy, including the seemingly simple approximation of $u^{+2}v^+=u^+(u^+v^+)$.



(a)



(b)

Fig. 4. (a) du^{+3}/dy budget for channel flows from Eq. 11; and (b) parametric variation zoomed in close to the wall. DNS data is from Graham et al. [11].

The above gradient can again be integrated to yield the spatial distribution of u^{+2} , by first finding u^{+3} then setting $u^{+2} = (u^{+3})^{2/3}$. The result is shown in Fig. 5. In spite of the close agreement in du^{+3}/dy , the integration is not so forgiving of any minute errors and results in deviation from the DNS data due to sharp peak and large gradient turns in the near-wall region. Moreover, these errors accumulate to cause departure from the centerline ($y/H=1$) boundary condition, when integrated starting from the wall ($y/H=0$). To correct for the numerical errors, we again enforce the centerline boundary condition, without the loss of integrity of the current approach, by setting $(u^{+2})_{\text{corr}} = (u^{+2})_{\text{integrated}} - c_u(y/H)$. The constant c_u is $=\Delta u^{+2}$ =deviation of the $(u^{+2})_{\text{integrated}}$ from u^{+2} at $y/H=1$. The result is shown below, where due to the above difficulty, there is some + and - deviations from the DNS data in the mid-flow region ($y/H=0.1 \sim 1$). Nonetheless, the result is not bad considering the difficulty of tracking the sharp peak and gradient changes in the u^{+2} profiles,

which tend to grow in severity with increasing Reynolds number in wall-bounded turbulent flows [12].

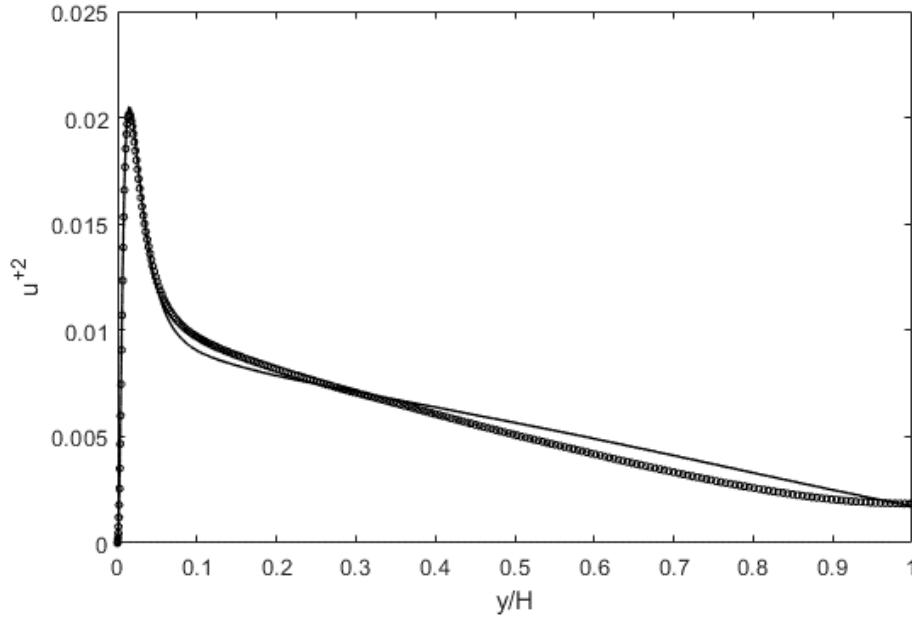
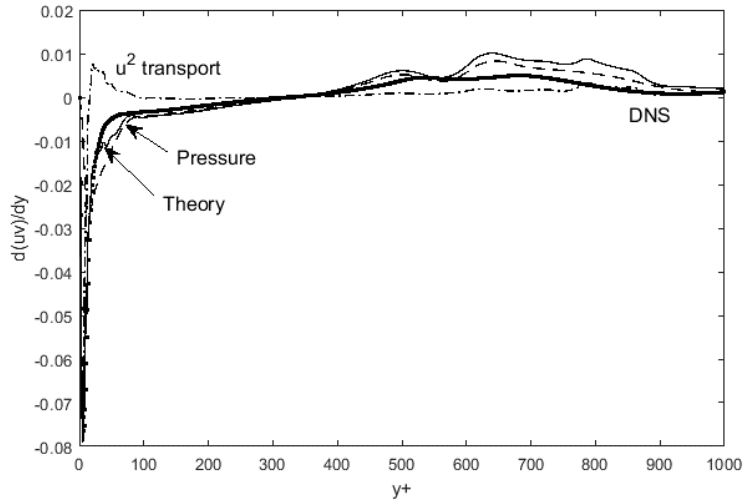


Fig. 5. Comparison of u^{+2} profile obtained from numerical integration of Eq. 11, with DNS data [11]. Boundary conditions are applied both at the wall ($y/H=0$) and the centerline ($y/H=1$).

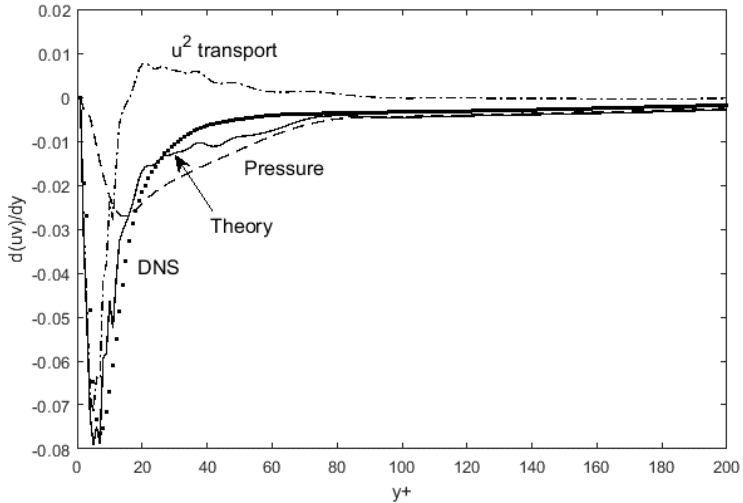
Applications in Other Flow Geometries

Now we compare Eq. 10 with the DNS data for adverse-pressure gradient boundary layer flows by Kitsio et al. [13], for $Re_{\delta_2} = 3500$, as shown in Fig. 6. Figs. 6(a) and (b) are the entire profile across the boundary layer and zoomed-in version for the near-wall region, respectively. We can see that the overall agreement between Eq. 10 and DNS results is good across the boundary layer; however, the undulations away from the wall is mimicked but not exactly followed by Eq. 10. This is due to the inaccurate tracing of the DNS data, leading to some errors when taking the gradient of the transcribed data. This kind of numerical differentiation errors is also evident in Figure 6(b) as well, where a close inspection of the near-wall region again shows that Eq. 1 tracks

the DNS data reasonably well, albeit with some small spikes and undulations. At the inflection point ($y^+ \sim 40$), there is some deviation from DNS data. Nonetheless, Figs. 6(a) and (b) provide some solid grounds for Eq. 10, where the adverse pressure gradient effect is manifest through the C_{12} term.



(a)



(b)

Fig. 6. Reynolds stress gradient budget for flow over a flat plate at zero pressure gradient. DNS data is from Kitsios et al. [13]. $Re_{\delta_2} = 3500$. (b) contains the same data as (a), except zoomed on the near-wall region.

After properly vectorizing the gradients and using the centripetal pressure, we see that the same logic of turbulence momentum transport is applicable in pipe flows with swirl, as shown in Fig. 7. DNS data of Nygard and Andersson [14] are used.

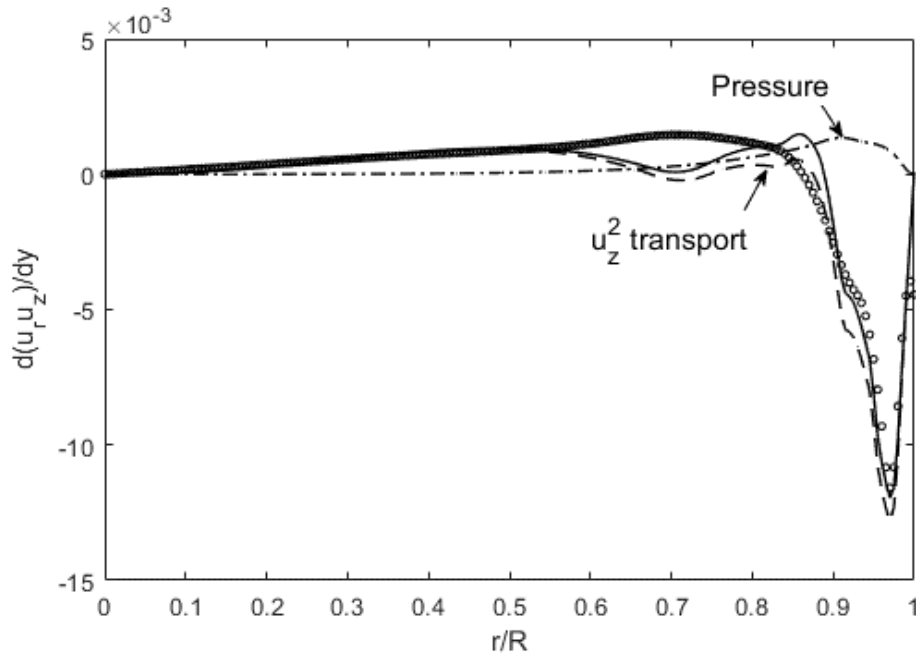


Fig. 7. Comparison of Reynolds shear stress gradient budget in pipe flows with swirl (Eq. 13) with DNS data [14].

Use of the Full Turbulent Transport Equations for Jet Flows

For jet flow with free ambient boundary conditions, the equations become yet simpler.

$$\frac{d(\overline{u'v'})}{dy} = C_1 U \frac{d(\overline{u'^2})}{dy} \quad (15)$$

$$\mu \frac{dU}{dy} = -\rho(u'v') \quad (16)$$

$$C_2 U \frac{d(\overline{u'^3})}{dy} = - \frac{d(\overline{u'^2 v'})}{dy} + 2\nu \left(\frac{du'_{rms}}{dy} \right)^2 \quad (17)$$

This allows for relatively simple numerical solution schemes. Although one was presented in Ref. 9, we describe an improved algorithm to solve the above set of equations. We start by an initial estimate of the u'^2 profile and its gradient. Structural constraint method is useful in coming up with this initial estimate, where knowing the peak location and the total energy content as a function of the Reynolds number is quite expedient in structural reconstruction of u'^2 profiles [12]. With this estimate, initial Reynolds shear stress and the mean velocity profile can be directly computed using Eqs. 15 and 16, respectively. The centerline boundary conditions, $U/U_o = 1$ and $u'v' = 0$ are used. Then, u'^2 profile can be updated using Eq. 17, and the process iterated until the freestream boundary conditions are reached for all variables. The converged results are compared with experimental data [15], in Figs. 8-10.

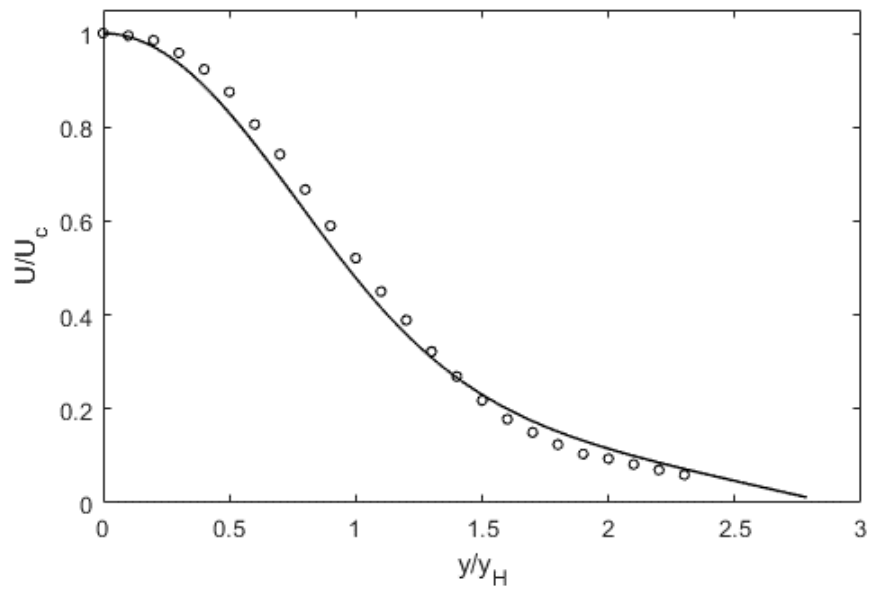


Fig. 8. Comparison of the mean velocity profile obtained from iterative numerical integration of Eqs. 15-17, with experimental data [15].

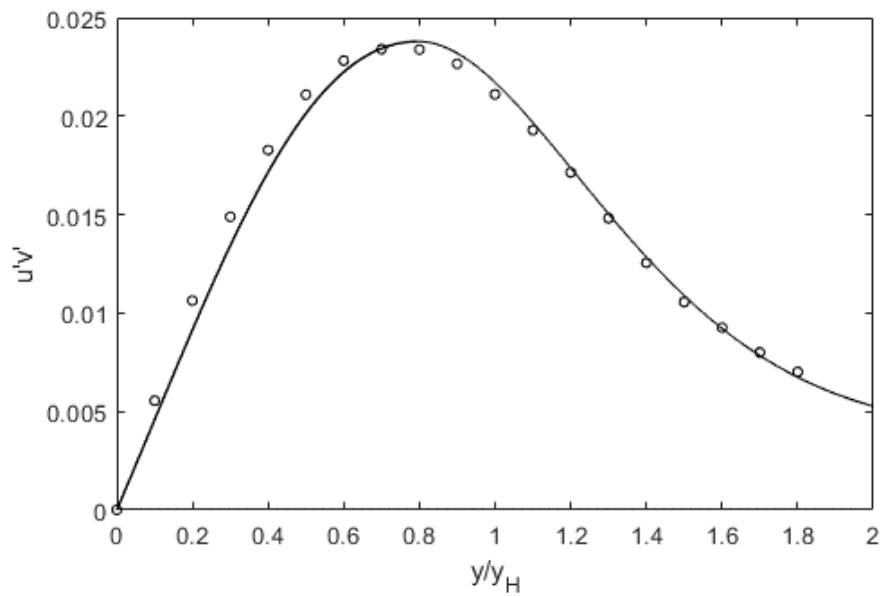


Fig. 9. Comparison of the Reynolds shear stress obtained from iterative numerical integration of Eqs. 15-17, with experimental data [15].

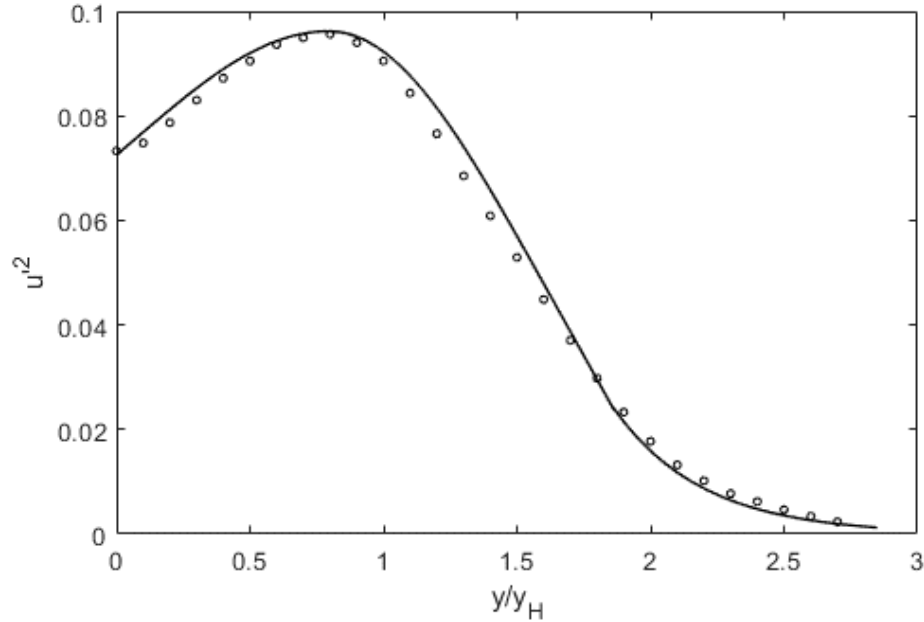


Fig. 10. Comparison of u'^2 profile obtained from iterative numerical integration of Eqs. 15-17, with experimental data [15].

CONCLUSIONS

Using the Lagrangian transport of momentum, the Reynolds shear stress can be expressed in terms of basic turbulence parameters. In this view, the Reynolds stress gradient represents the lateral transport of streamwise momentum, balanced by the u'^2 transport, pressure and shear force terms in the momentum equation. We extend this formalism to other turbulence parameters such as diagonal components of the Reynolds stress, and also to other geometries (boundary layer flows with adverse pressure gradients and pipe flows with swirl). Data from direct numerical simulations (DNS) are used to validate this full set of turbulent transport equations, exhibiting a good degree of consistency and agreement for all of the components and across different geometries. An

example of the use of this full set of turbulence transport equations is shown for turbulent jet flows. This formalism is based on the Lagrangian turbulence transport, and therefore is fundamentally generalizable to other flow configurations. The resulting terms reproduce the main turbulence variables, while revealing the internal dynamics linking these components.

APPENDIX

Probe Transform

For channel flows, the flow is bounded and there is no displacement of the turbulence variables as one travels in the streamwise direction. However, the Galiean transform can be performed at any line of motion, and if we choose a slightly mis-directed path (U^* and v^*) for the control volume as shown in Figure A1, we obtain the same transform as shown below. In Figure A1, x^* and y^* axes are aligned in the same direction as U^* and v^* , respectively.

For a small angle, $\theta \ll 1$, $v^* \ll U$ and $U^* \approx U$. Then,

$$\frac{\partial}{\partial x} = \frac{1}{\cos\theta} \frac{\partial}{\partial x^*} \approx \frac{\partial}{\partial x^*} \quad (\text{A1})$$

$$\frac{\partial}{\partial y} = \frac{1}{\cos\theta} \frac{\partial}{\partial y^*} \approx \frac{\partial}{\partial y^*} \quad (\text{A2})$$

For variable, f , we have

$$\frac{\frac{\partial f}{\partial y^*}}{\frac{\partial f}{\partial x^*}} \approx \frac{\frac{\partial f}{\partial y^*}}{\frac{\partial f}{\partial x^*}} = \tan\theta = \frac{v^*}{U^*} \approx \frac{v^*}{U} \quad (\text{A3})$$

Thus, using this offset transform, we obtain

$$\frac{\partial f}{\partial x} = \frac{U^*}{v^*} \frac{\partial f}{\partial y} \approx C_1 U \frac{\partial f}{\partial y} \quad (\text{A5})$$

C_1 is a constant in the order and unit of v^* .

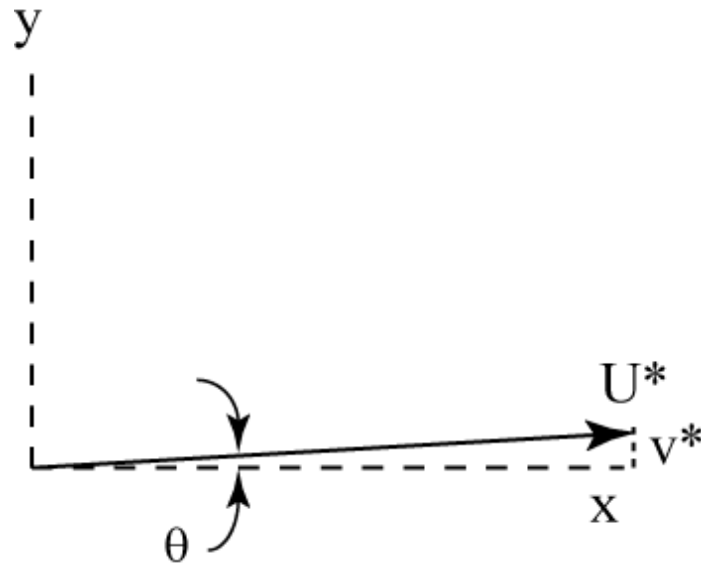


Figure A1. Off-set line of motion for the control volume, for “probing” the d/dy gradient.

REFERENCES

- [1] Launder, B.E., Reece, G.J., and Rodi, W., Progress in the development of a Reynolds-stress closure, *Journal of Fluid Mechanics*, 1975, Vol. 68, Part 3, pp. 537-566.
- [2] Mansour, N.N., Kim, J. and Moin, P., Reynolds-stress and dissipation-rate budgets in a turbulent channel flow, *Journal of Fluid Mechanics*, 1988, Vol. 194, pp. 15-44.
- [3] Hanjalic, K., Advanced turbulence closure models: a view of current status and future prospects, *Int. Journal of Heat and Fluid Flow*, Vol. 15, No. 3, 1994, pp. 178-203.
- [4] Pope, S. B., Simple models of turbulent flows, *Physics of Fluids*, 2011, 23, 011301.
- [5] Hamba, F., Exact transport equation for local eddy viscosity in turbulent shear flow, *Physics of Fluids*, 2013, 25, 085102.
- [6] Inagaki, K., Ariki, T., and Hamba, F., Higher-order realizable algebraic Reynolds stress modeling based on the square root tensor, 2019, arXiv:1905.06106v2.

- [7] Lee, T.-W., Reynolds stress in turbulent flows from a Lagrangian perspective, *Journal of Physics Communications*, 2018, 2, 055027.
- [8] Lee, T.-W., and Park, J.E., Integral Formula for Determination of the Reynolds Stress in Canonical Flow Geometries, *Progress in Turbulence VII* (Eds.: Orlu, R, Talamelli, A, Oberlack, M, and Peinke, J.), pp. 147-152, 2017.
- [9] Lee, T.-W., Lagrangian Transport Equations and an Iterative Solution Method for Turbulent Jet Flows, *Physica D*, 2020, 132333.
- [10] Pope, S. B., *Turbulent Flows*, Cambridge University Press, 2012.
- [11] Graham, J., Kanov, K, Yang, X.I.A., Lee, M.K., Malaya, N, Lalescu, C.C., Burns, R., Eyink, G, Szalay, A, Moser, R.D., and Meneveau, C., A Web Services-accessible database of turbulent channel flow and its use for testing a new integral wall model for LES, *Journal of Turbulence*, 2016, 17(2), 181-215.
- [12] Kitsios, V, Atkinson, C, Sillero, J.A., Borrell, G, Gungor, A.G., Jiménez, J., and Soria, J, Direct numerical simulation of a self-similar adverse pressure gradient turbulent boundary layer , *International Journal of Heat and Fluid Flow*, 2016, 61, 129–136.
- [13] Lee, T.-W., Maximum entropy method for solving the turbulent channel flow problem, 2019, *Entropy*, 21(7), 675.
- [14] Nygard, F. and Andersson, H., DNS of swirling turbulent pipe flow, 2009, *International Journal of Numerical Methods in Fluids*, 64 (9), pp. 945-972.
- [15] Gutmark, E. and I. J. Wygnanski, The Planar Turbulent Jet, *Journal of Fluid Mechanics*, 1970, Vol. 73, Part 3, pp. 466-495.